Journal of the Optical Society of America B
OPTICAL PHYSICS

Growth of terahertz surface plasmon propagation length due to thin-layer dielectric coating

Vasily V. Gerasimov,[1,2,*] Boris A. Knyazev,[1,2] Alexey G. Lemzyakov,[1] Alexey K. Nikitin,[2,3] and Guerman N. Zhizhin[3]

[1]Budker Institute of Nuclear Physics SB RAS, 11 Lavrentyev Avenue, Novosibirsk 630090, Russia
[2]Novosibirsk State University, 2 Pirogova Street, Novosibirsk 630090, Russia
[3]Scientific and Technological Center for Unique Instrumentation of RAS, 15 Butlerova Street, Moscow 117342, Russia
*Corresponding author: einy@ngs.ru

Received 26 July 2016; revised 8 September 2016; accepted 8 September 2016; posted 13 September 2016 (Doc. ID 272278); published 5 October 2016

Here we consider a longstanding problem: why terahertz (THz) surface plasmons (SPs) do not run so far as the Drude theory predicts. We experimentally demonstrated that the main cause for this paradox was a drastic rise in the SP radiative losses at THz frequencies, not violation of the theory. Analysis of SPs induced with the radiation of the Novosibirsk free electron laser ($\lambda = 130\ \mu$m) showed that a thin dielectric layer ($\approx \lambda/250$) on a metal surface can reduce the losses substantially and hence enlarge the SP propagation length several times. Furthermore, it was found that there was an optimal layer thickness corresponding to the minimum total SP energy losses; the cause of this phenomenon is discussed.

OCIS codes: (240.6680) Surface plasmons; (240.6700) Surfaces; (260.3090) Infrared, far; (290.5880) Scattering, rough surfaces.

http://dx.doi.org/10.1364/JOSAB.33.002196

1. INTRODUCTION

Surface plasmons (SPs), a kind of *p*-polarized electromagnetic evanescent wave capable of propagating along a metal/dielectric interface, are widely used in optical devices in the visible and infrared (IR) spectral ranges [1,2]. SP characteristics (propagation length L, depth of field penetration in air δ, phase velocity, and others) measured in these ranges are in good accord with those calculated by the Drude model for the dielectric permittivity of metals [3,4]. Moreover, the measured L values are proportional to the second power of the wavelength (λ), which confirms the applicability of the model in these spectral ranges [5].

The situation changes in the far IR, particularly in the terahertz (THz) range. First experiments with SPs excited by far IR gas lasers revealed great discrepancy between the calculated and measured L values on bare metal surfaces. In the experiments, THz SPs ran distances 2 orders smaller than those predicted by the theory: instead of several meters calculated for a perfect plane interface, real THz SPs ran only a few centimeters [6,7]. The same results were obtained when THz SPs were generated by free electron lasers [8,9] or by *ps* broadband pulses of light spanning the whole THz spectral range (the time-domain spectroscopy technique) [10–12]. The proportion of $L \sim \lambda^2$ is violated somewhere between the middle and far IR ranges; the cause remained unclear for decades. Some researchers [9,12] suppose that the most probable cause of these discrepancies is a distinction in the dielectric properties of real metal surface and respective bulk crystal. This hypothesis has not found a clear experimental confirmation so far. Another explanation of the great attenuation of THz SPs can be the "radiative" losses of SPs on the roughness and intrinsic inhomogeneity of the surface. At first sight, as the dimensions of optical surface roughness are usually negligible in comparison with a THz radiation wavelength, the radiative losses cannot give rise to a considerable attenuation of THz SPs. However, one has to take into account the small difference between the THz SP wave vector and that of plane waves in free space; it may lead to intensive SP conversion into bulk waves (BWs), even on tiny surface imperfections.

So, we decided to investigate more thoroughly the influence of the radiative losses of THz SPs on their attenuation along real plane metal/dielectric interfaces. First, we detected the bulk radiation emitted by SPs from their track and determined the radiation pattern of these BWs. Second, it was very desirable to find a way to reduce the losses in order to enlarge the SP propagation length, which is of great importance for building lengthy THz SP communication lines and plasmonic integrated circuits [13].

2. BRIEF THEORY AND NUMERICAL ESTIMATIONS

SPs are inherently nonradiative surface waves because the real part k'_{SP} of their wave vector $k_{SP} = k'_{SP} + i \cdot k''_{SP}$ (where i is the

imaginary unit) exceeds the wave vector $k_0 = \omega/c$ of a plane wave in free space (where ω is the cyclic frequency and c is the speed of light in vacuum). However, when the guiding interface has roughness or intrinsic impurities, SPs lose their nonradiative nature, and thus acquire additional losses, referred to as "radiative" due to their origin [14]. Imperfections of the surface add an increment $\Delta k = \Delta k' + i \cdot \Delta k''$ to the wave vector k_{SP}. Note that the value of Δk is not strictly defined; it is distributed over a relatively large span, reaching a maximum in its center. If $\Delta k'$ is negative (in case the SP wave vector $\boldsymbol{k}_{SP}$ and the imperfection impact $\Delta \boldsymbol{k}$ are oppositely directed), it may result in the inequality

$$k'_{SP} - |\Delta k'| < k_o, \quad (1)$$

thus making the SPs radiative and running a shorter distance as compared with the case of ideal plane interface. In the visible range, the dispersion curve $k_{SP}(\omega)$ is spaced from the light line $k_0(\omega)$ by a rather large distance (along the k-axis) mainly exceeding the maximal value of possible $\Delta k'$, which results in relatively small radiative losses of the SPs. However, with an increase in λ, the dispersion curve comes closer and closer to the light line, making the transformation of SPs into BWs on surface imperfections more and more probable. This means that at low frequencies, particularly in the THz range, the role of radiative losses in total SP attenuation on a real interface is expected to increase. This increase may indeed be the main cause of the discrepancy between the calculated and measured SP propagation lengths at THz frequencies in spite of the fact that the intensity of SP radiative losses on surfaces with Gaussian roughness correlation function is proportional to the $1/\lambda^5$ [14]. For microscopic roughness in the long-wave range, the radiative losses must be negligible, but in case of a macroscopic roughness, it can be substantial.

Searching for a way to reduce the THz SP radiative losses, we suggested covering the metal surface with a thin dielectric layer of thickness $d \ll \lambda$. The point is that a layer on the guiding surface can increase the SP wave vector k_{SP} (or the SP complex refractive index $\kappa = \kappa' + i \cdot \kappa' = k_{SP}/k_0$) so that the most probable value of $\Delta k'$ will be insufficient to satisfy inequality [Eq. (1)], and no considerable reduction in the SP radiative losses will take place.

As an example, let us consider SPs with $\lambda = 130$ μm propagating along a gold surface covered with a zinc sulfate (ZnS) film of thickness d and obtain the dependence of κ' on d. To do this, we need to solve the dispersion equation for SPs in a three-layer structure [1,2], substituting the following parameters: the ZnS refractive index $n_2 = 2.95 + i0.01$ [15], the air refractive index $n_3 = 1.0002726$ [16], and the dielectric permittivity of the metal ϵ calculated by the Drude model with the damping frequency $\nu\tau = 215$ cm^{-1} and the plasma frequency $\nu p = 72,800$ cm^{-1} for gold [17]. The calculated dependence of $(\kappa' - n_3)$ on d in the range $0 < d < 1$ μm is displayed in Fig. 1. Note that the curve starts not from the zero ordinate but from the point $(\kappa' - n_3) = 6 \times 10^{-7}$, corresponding to SPs on a bare gold surface. It is believed that if the increment $\Delta k'$ caused by surface imperfections makes the difference $(\kappa' - n_3) = [(k'_{SP} - \Delta k')/k_o - n_3]$ belong to the region limited by the curve and the d-axis in Fig. 1, the radiative losses

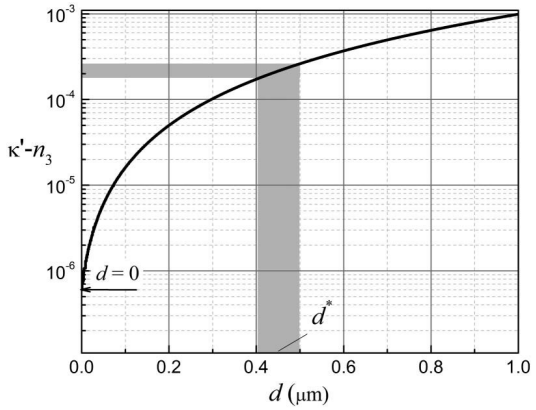

Fig. 1. Value of $(\kappa' - n_3)$ versus d calculated for "Au—ZnS layer of thickness d–Air" structure at $\lambda = 130$ μm. Dashed lines indicate the layer thickness d^* at which the SP propagation length L along the experimental structures reaches maximum (see Section 4.B).

of the SPs are reduced by far (not eliminated completely though, due to an uncertainty in $\Delta k'$).

On the other hand, it is a well-known fact that a dielectric layer on a metal surface causes SP field redistribution, leading to an increase in the field portion carried inside the metal, and thus reducing the SP propagation length [18–20]. Thus, one may conclude that with growth of the coating layer thickness d two competitive processes, determining the SP propagation length, take place: an increase of the Joule losses and a reduction of the radiative losses. In case the latter prevails over the former, the propagation length should increase with d-growth. We tested this hypothesis experimentally at the Novosibirsk free-electron laser (NovoFEL) [21], generating monochromatic THz SPs on flat glass samples covered with an opaque gold film and ZnS layers of various thickness.

3. EXPERIMENTS

A. Experimental Setup

The experimental schematic is shown in Fig. 2. A p-polarized Gaussian beam of the NovoFEL with a waist of 15 mm and a wavelength of 130 μm entered the experimental setup as a continuous stream of 100-ps pulses with a 5.6 MHz repetition rate and an average power of about 10 W. Polarizers Pol 1 and Pol 2 were applied for beam attenuation and polarization control, accordingly. The input beam intensity was monitored using a beam splitter (BS) with a pyroelectric sensor.

To transform the bulk radiation into SPs, instead of a parallel plate waveguide used in previous investigations [22], we employed the end-fire coupling technique [23] as a simpler, more effective, and more reliable method. In contrast to the classical implementation of the method with a rectangular edge of sample, we used a one-eighth part of a glass cylinder (see Fig. 2), its optical-quality polished curved surface covered with a 1-μm thick gold film as a coupling element [24]. The cylindrical form of the coupling element made it an effective screen, shielding the photodetector from diffracted BWs. The radius of the cylinder, $R = 60$ mm, exceeded λ manifold, which made the curvature contribution to the radiative losses negligible

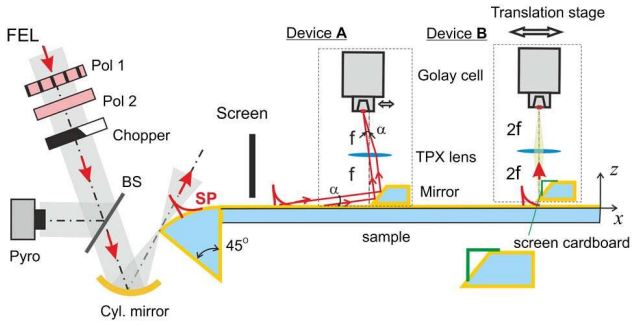

Fig. 2. Experimental setup with the end-fire coupling technique to excite SPs on the edge of a cylindrical coupling element attached to a plane-surface sample: device A, for sensing SP radiative losses; device B, for measuring the SP field penetration depth δ (decay length) in air and the SP propagation length L.

[25]. To increase the coupling efficiency, we covered the gold film of the coupling element with a ZnS layer 2 μm thick. The generated SPs proceeded from the cylindrical surface of the coupling element to the sample plane surface adjoining it.

To study the THz SP field distribution along the track, we employed two devices: A and B, used alternatively, not simultaneously (Fig. 2).

To measure the SP radiative losses, we used device A. BWs emitted from the track due to the interaction of the SPs with surface imperfections were reflected by a 45° inclined plane mirror and detected with a TPX lens and an optoacoustic detector (a GC-1D Golay cell with NEP 1.4×10^{-10} W/Hz 1/2. The Golay cell was coupled to a lock-in amplifier (SR-830) tuned at a 15 Hz chopping frequency. The mirror, the detector, and the lens were placed on an optical rail in f-f arrangement, where $f = 100$ mm is the focal length. The detector was equipped with a 0.2 mm diaphragm (oriented normally to the plane of incidence), cutting off parasitic BWs. In addition, the detector was shielded with an accessory metal screen from BWs generated by the SPs due to their diffraction on the junction between the coupling element and the sample. The diffraction was caused by the not ideal contact and difference in ZnS layer thickness on the coupling element and the sample [26]. The screen was fixed over the SP track, its edge 15 mm from the junction and 10 mm from the sample surface. The focusing lens transforms the incoming radiation into the spatial Fourier-spectrum in the focal plane. Scanning the detector in the focal plane along the x-axis, we recorded the angular patterns of bulk radiation emitted by the SPs due to their interaction with the surface imperfections (see Section 4.A).

The device B was used for determination of the SP propagation length L and the decay length in air δ (see Section 4.B). Running along a sample surface, SPs stroke against the same plane mirror; this again resulted in the decoupling of the SPs into BWs. However, this time a negative increment in the SP wave vector, necessary for the SP decoupling, was obtained in the process of the SP diffraction on the mirror edge. The complex "TPX lens–Golay cell" arranged now in $2f$-$2f$ (with $f = 50$ mm) imaging scheme, which enabled us to visualize exclusively the mirror edge (not other points of the mirror reflecting facet). To screen the detector from radiative waves and BWs produced by the SPs diffracting on the junction, the reflecting facet of the mirror was covered by a thick cardboard, as shown in Fig. 2. The cardboard almost did not cut BWs produced by diffracted SPs on the mirror edge, as the diffraction pattern of SPs was narrow (≈4°). To measure the SP field distribution, we placed the mirror and the detection complex on a translation stage movable both along the SP track (x-axis) and along the normal (z-axis) to the guiding surface, which enabled recording the distribution of the SP field intensity in those directions.

B. Samples

We prepared two sets of samples, which were thick glass bars 15 cm long, 3.5 cm wide, and 1 cm thick with flat polished upper faces. The samples of the first set, further referred to as "imperfect" ones, were polished with low quality, covered with a thermally evaporated gold film 1 μm thick, and optionally coated with a thermally evaporated ZnS layer 0–3 μm thick. The better quality samples, referred to as "perfect" ones, were optically polished, covered with gold films 0.3 μm thick by DC magnetron sputtering and optionally coated by e-beam evaporation with a ZnS layer of that or another thickness. The gold film could be considered as a semi-infinite medium in our case, as according to the Drude model the skin depth in gold at THz frequencies is about 44 nm, while the electron free path is 41 nm, which is substantially smaller than the film thickness.

We examined the sample surfaces with an atomic force microscope (AFM) in the semicontact regime. Images of 1 μm × 1 μm square areas of the surfaces are shown in Fig. 3. On the bare gold surfaces for both sets of samples [see Figs. 3(a) and 3(b)] one can clearly see a granular structure, which is typical of evaporated thin gold films [27]. Processing the images numerically, we obtained several characteristics of the surfaces, which are important for SP attenuation study (see Table 1). The sample ZnS layer thicknesses d were measured by the ellipsometric technique. Deviations of d values from their mean value over a 150 mm distance along the sample surface are written in the last column of Table 1. Analysis of these results reveals that (1) the microscopic RMS roughness of the "perfect" samples was significantly less than that of the "imperfect" ones; (2) the bare gold surfaces of both sets of samples had a regular granular structure, but the mean grain diameter of the "perfect" samples was about twice as small as that of the "imperfect" ones; (3) the mean grain diameter and height were comparable with the electron-free path in gold, which could decrease the

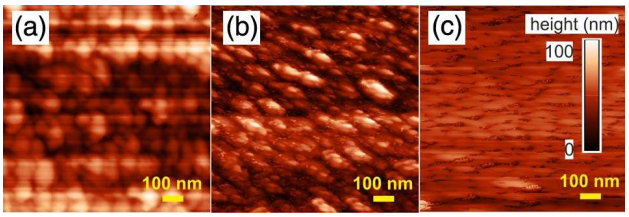

Fig. 3. AFM images of 1 μm × 1 μm areas of sample surfaces with (a) 1-μm bare gold film thermally evaporated on imperfectly polished glass substrate; (b) 0.3-μm bare gold film evaporated on perfectly polished glass substrate by magnetron sputtering; (c) 0.3-μm gold film covered with ZnS layer 0.52 μm thick.

Table 1. Characteristics of Sample Surfaces Measured with an AFM

Samples	Mean Grain Diameter, nm	Mean Grain Height, nm	RMS Roughness (Over 100 μm × 100 μm Area), nm	ZnS Layer Thickness Deviation (Over 150 mm Distance), nm
"Imperfect"	75 ± 30	20	50	20
"Perfect"	30 ± 20	30	20	10

effective dielectric permittivity of the metal surface as compared with that of the bulk metal; and (4) the ZnS layer thickness of the "perfect" samples was more uniform. Additional testing of ZnS layers with an electron microscope revealed a high clarity and uniformity of their content for both series of samples.

Imperfections caused by the ZnS coating grains (see Table 1) and deviations of ZnS layer thickness are too small to produce substantial radiative losses. Therefore coverage of the metal surface with a dielectric film made the SPs-BWs transformation process less probable, due to a shift of the SP dispersion curve from the light line (see Section 2).

4. EXPERIMENTAL RESULTS AND DISCUSSION

A. Direct Sensing of Bulk Radiation from SP Track

The most crucial evidence of the existence of SP radiative losses was the direct sensing of BWs emitted from the track due to the SP conversion on surface imperfections. To carry out measurements of this kind, we used the setup shown in Fig. 2 (device A). Scanning the detector along the x-axis in the focal plane of the lens, we measured the angular spectrum $I(\alpha)$ of the radiation coming from the reflecting facet of the mirror, where angle $\alpha = \text{arctg}(x/f)$. The edge of the mirror was put on the sample surface at the distance $x \approx 150$ mm from the "coupling element–sample" junction. The angular distributions of the incoming radiation recorded for the "perfect" samples containing ZnS layers of thickness $d = 0.0$, 0.4, and 0.7 μm are shown in Fig. 4. Each individual diagram recorded for a given sample had two main maxima (a subsidiary maximum was observed only for the sample with $d = 0.70$ μm).

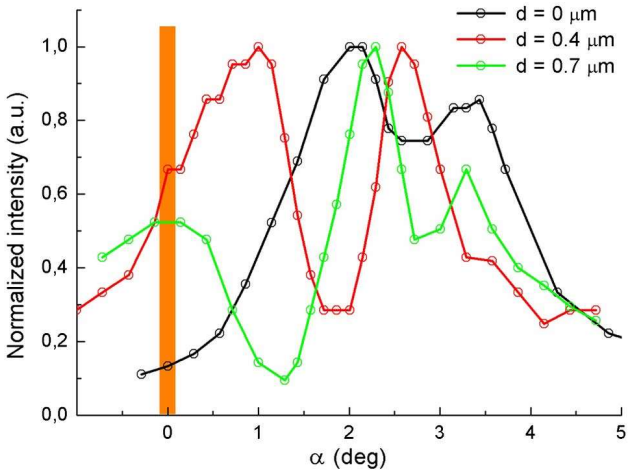

Fig. 4. Radiation patterns recorded from SP track on Au samples (set of "perfect" samples) with ZnS layer of various thicknesses d using 45° inclined mirror placed normally to the track (see schematic A in Fig. 2).

The first maximum, observed in the angular span $\alpha = (0–2)°$, where α is either the angle counted from the sample surface to the BW wave vector or the angle of the BW incidence onto the Golay cell entrance window, as well as the third one for the sample with $d = 0.70$ μm at $\alpha \approx 3.5°$, corresponded to BWs produced by the SPs due to their diffraction on the edge of the mirror. Note that the thicker the ZnS layer, the closer is the SP maximum (the first one) to the normal ($\alpha = 0°$). Similar radiation patterns were observed with SPs diffracting on a sample rectangular edge [22], which is evidence of the diffractional nature of the SP transformation on the mirror edge.

The second maximum (at a greater α) was formed by BWs produced by the SPs on their track due to interaction with surface imperfections. To make sure that the second maximum was really produced by BWs incident on the 15-mm long reflecting facet of the mirror and that it had a "radiative" nature, we tested the maxima using two paper strips.

First, we put a paper strip 1 (10 mm wide) on the SP track. When the strip was between the metal screen and the mirror, the first maximum decreased about two times (at any place on the track), while the second maximum remained unchanged. When the strip 1 moved closer to the junction between the coupling cylinder and the sample, the second maximum gradually decreased. This evidenced the "plasmon" nature of the first maximum and the "radiative" nature of the second one. Reduction of the second maximum in case the strip was close to the junction corresponded to more powerful radiative waves emitted from the initial part of the track and absorbed by the paper.

Further, we put paper strip 2 (2.5 mm wide) on the 45°-mirror reflecting facet and moved it gradually downward to the sample surface (see Fig. 5). Below we describe the observed changes in the maxima when the strip was being moved downward to the sample with a ZnS layer 0.40 μm thick. As soon as the strip was put on the upper edge of the facet of the mirror,

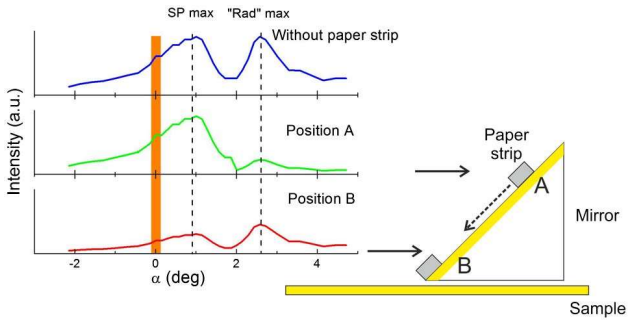

Fig. 5. Testing "radiative" nature of the second maximum with a paper strip 2: experimental scheme and results for the sample with ZnS layer 0.4 μm thick.

the second maximum started decreasing, and when the strip passed one-third of the facet length (position A in Fig. 5), its intensity was four times as small as the initial value. Up to this position, the first SP maximum remained unchanged. Further shifting of the strip toward the lower edge of the mirror led to a gradual increase in the second maximum and a decrease in the first one. At the terminal point of the strip motion, when it touched the sample surface (position B in Fig. 5), the second maximum was half of its initial value, while the first maximum reached its minimum, about one-third of its initial value. Such behavior of the maxima evidences the existence of BWs emitted from the SP track and propagating at an angle α with the sample surface. Besides, the radiative waves were indicated in the whole tested angular span ($\alpha \approx 0$–$4°$), with their intensity reaching its top at the second maximum. This means that the radiative waves had a wide angular spectrum. It is worth noting that with the ZnS layer thickness growing, the second maximum shifts to the normal ($\alpha = 0°$) like the first one, which indicates an increase in the SP wave vector with thicker coatings.

To make sure that the observed maxima were not produced by parasitic BWs originated due to the SP diffraction on the junction, we made similar experiments employing the waveguide coupling technique on samples with an inclined edge (see [22]). Such a schema excludes a junction between the coupling element and the sample. Still, we observed the same maxima, and their testing gave the results similar to those described above. So, almost total elimination of parasitic BWs brought no new results and confirmed existence of radiative losses.

B. Measurements of SP Decay and Propagation Length

To test our hypothesis about possible reduction in the SP radiative losses due to a dielectric coating, we measured the distribution of SP field intensity I (see Fig. 2, scheme B) both along the track (x-axis) and along the normal to the surface (z-axis) with both sets of samples. First, we measured the I-distribution along the z-coordinate. As an example, the experimental dependence $I(z)$ measured for the sample with $d = 0.4$ μm is presented in Fig. 6. The intensity decreased exponentially in accordance with the theory of SPs. Besides, quite in line

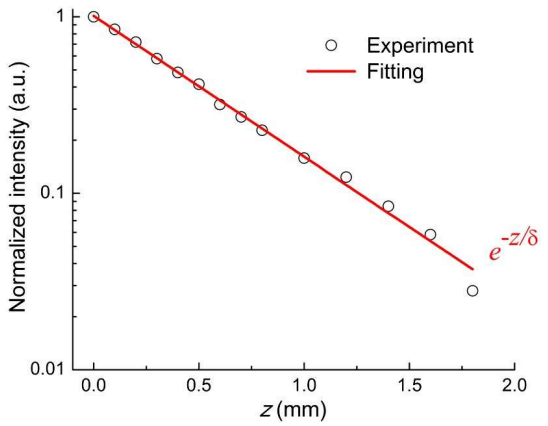

Fig. 6. SP intensity versus z-coordinate recorded for the sample with ZnS layer 0.4 μm thick.

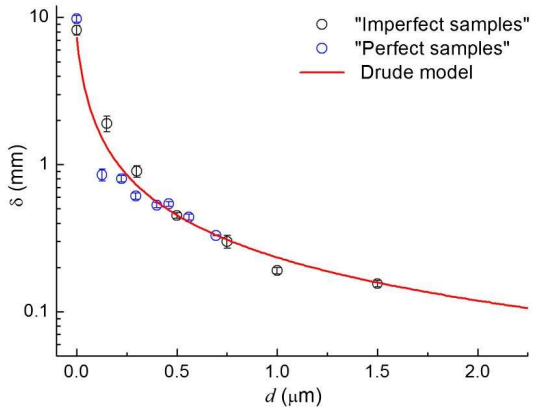

Fig. 7. Decay length δ of SP field into air versus ZnS layer thickness d: experimental data for "imperfect" and "perfect" sets of samples (circles); calculations (solid line).

with the theory, we noted that the thicker the ZnS layer, the more compact was the distribution of SP field over the guiding surface. The length of SP field decay in air δ (the distance at which the SP field intensity drops by a factor of $e \approx 2.718$) derived from the experimental dependences decreasing monotonically with d increase (Fig. 7). The experimental results for both sets of samples agree well with δ values calculated by the Drude model for the dielectric permittivity of metals. This accordance is evidence of the classical model applicability for gold in the THz region.

At the same time, we have to admit that these results disagree to some extent with predictions of the theory developed in [28], which states that, in case of a rough metal-air interface with a roughness characterized by a Gaussian correlation function, SP decay length δ values must be about two times less than Drude theory predicts and their radiative losses cannot cause the experimentally observed significant reduction of the SP propagation length [30]. Nevertheless, as noted in [28], the actual correlation function of a rough surface may differ from the Gaussian one and, in case of a nonmonotonic correlation function, the effect of SP radiation losses could be enhanced.

In the next stage of measurements, we recorded the dependences $I(x)$, the 45°-mirror with the detection system (see Fig. 2, device B) being moved along the SP track on the translation stage with a 10-mm step. At each measurement point, the mirror was put down onto the sample surface. The results obtained for the "imperfect" samples are shown in Fig. 8. The experimental points for any given sample can be well approximated with an exponential curve. Note that the uppermost curve, corresponding to the smallest attenuation of the SPs, is not for $d = 0$ but for d belonging to the interval from 0.15 to 0.75 μm. To determine the optimum d^* value, at which the propagation length attains its maximum, we calculated the dependence $L(d)$ (see Fig. 9) via exponential fitting of the experimental curves $I(x)$. To compare the experimental dependence $L(d)$ with that calculated by the Drude model, we plotted them both in the inset of Fig. 9. The error bars' size was supposed to be equal to 10% from the corresponding value of L, and was mainly determined by the laser radiation stability. One can see that the L value measured for bare gold

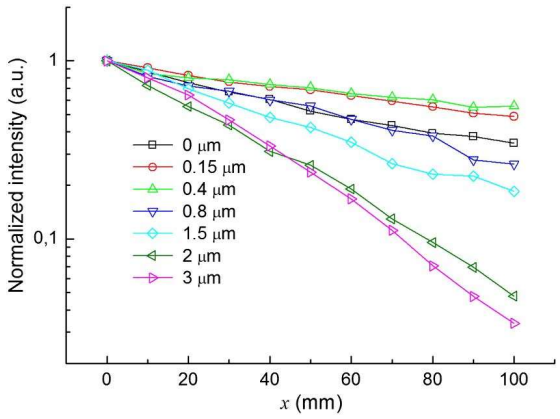

Fig. 8. SP normalized intensity versus distance x run by surface wave along "imperfect" samples with ZnS layers of different thicknesses d.

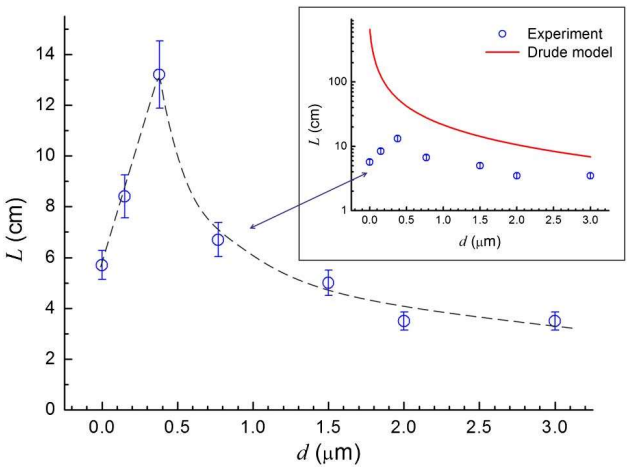

Fig. 9. SP propagation length L estimated from plots in Fig. 8 versus ZnS layer thickness d ("imperfect" samples). Inset: same experimental values L (circles) along with curve calculated by Drude theory (solid line).

($d = 0$) is about 2 orders less than the calculations predict. This discrepancy gradually decreases as the ZnS layer thickness d goes up. Other investigators [18,19] noted this fact as well. We have to admit that L values obtained in the experiments under discussion are several times larger as compared with those determined in our previous experiments with different gold samples [22]. One of the causes of this discrepancy can be the different quality of the surface of the samples used in the series of experiments.

One can see that the experimental dependence $L(d)$ in Fig. 9 reaches its maximum $L_{max} \approx 130$ mm at $d* \approx 0.4$ μm, which is about two times larger than $L \approx 60$ mm for the bare gold surface. This fact is in accord with the above assumption that a dielectric coating on a surface may enlarge the SP propagation length due to some decrease in the radiative losses (see Section 2). The assumption is also backed up by the monotonic character of the plot $\delta(d)$ in Fig. 7. It indicates that the portion of the SP field carried inside the metal increases with d growth, which is expected to result in a corresponding rise in the SP attenuation caused by the Joule losses [2,18,19]. However, our experiments demonstrated that the SP attenuation, on the contrary, decreased with d growth, until it reached 0.4 μm value. However, for samples with $d > 0.5$ μm, the experimental L values decrease with d growth monotonically, as does the calculated curve, though the former is about two times lower than the latter for any d.

Combining the results obtained in the experiments (Fig. 9) and those calculated for the "Au–ZnS layer–Air" structure (see Fig. 1), one may state that the most probable negative increment $\Delta k'$ in the SP wave vector, originating from the surface imperfections, corresponds to $(\kappa' - n_3) \approx 1.7 \times 10^{-4}$, when the propagation length L reaches its maximum, while the SP total losses (the radiative plus the Joule ones) attain their minimum

We performed one more series of the experiments described above with the set of "perfect" samples, the surfaces of which were processed with higher quality. The samples had the same configuration and size, but the Au films deposited on their surfaces were coated with ZnS layers of thicknesses of 0, 0.072, 0.22, 0.3, 0.4, 0.52, 0.7, 2.0, and 3.6 μm. To increase the accuracy of the measurements, we moved the translation stage along the x-axis with the Golay cell automatically with a scanning pitch of 0.4 mm. In the scanning, the gap between the mirror and the sample surface was about 0.15 mm. The pass was 50 mm long. Examples of the newly measured dependences $I(x)$ are presented in Fig. 10. It is clearly seen that for the 3.6 μm thick ZnS layer, there are oscillations corresponding to interference between the BWs produced due to the SPs diffraction and the BWs radiated from the track. The interference effect is more pronounced for larger d, which can be related to smaller angles α of the radiative BWs for thicker dielectric layers (see Fig. 4).

Approximating the experimental points with exponential curves, we plotted one more $L(d)$ graph, shown in Fig. 11. The error bars' size was supposed to be equal to 10% from the corresponding value of L, and was mainly determined by the NovoFEL radiation stability. It is seen that refinement of the surface increased the propagation length L for all samples and almost did not have an effect on the d value at which the L value reached its maximum: the largest L value was attained at $d* \approx 0.5$ μm. This means that the microscopic surface

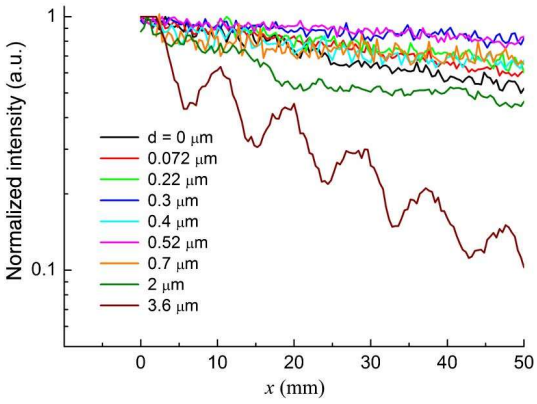

Fig. 10. SP intensity versus distance x measured with the set of "perfect" samples with ZnS layers of different thickness d.

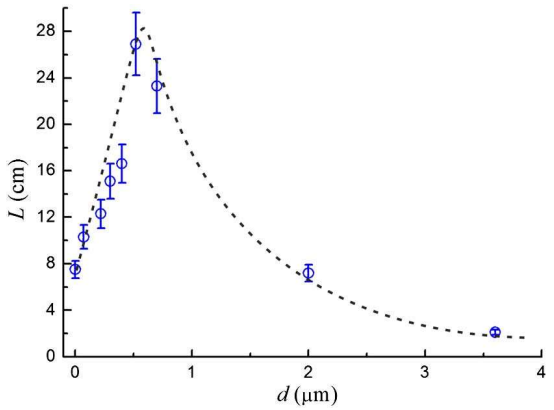

Fig. 11. SP propagation length L estimated from plots in Fig. 10 versus ZnS layer thickness d (set of "perfect" samples). Dashed line: approximation curve.

roughness of the samples (see Table 1 in Section 3.B) has no effect on the SP propagation length and cannot produce substantial radiative losses, as was mentioned in Section 2. But still, the dependence $L(d)$ had a peak, and the maximum L considerably (3.5 times) exceeded the L value on the bare sample.

Summarizing this paragraph, we would like to emphasize once again that results obtained in the described experiments contradict to some extent the classical SP theory for plane structures with ideal interfaces, which states that covering a metal substrate with a dielectric film is expected to decrease the L value (at least for films with $d < \lambda/10$) [18,19]. Meanwhile, we experimentally observed that the SP propagation length L increased with deposition of a thin ($d \approx \lambda/250$) dielectric layer on the metal surface. A reasonable explanation of this phenomenon can be given with a hypothesis that the layer along with a redistribution of the SP field from air into the metal (which raises the Joule losses) increases the SP wave vector as well, which results in a reduction in the radiative losses. Moreover, the maxima observed in the experimental dependences $L(d)$ indicate that in case the metal surface is covered with a thin dielectric layer, the reduction in the SP radiative losses prevails over the rise in the Joule losses. With a certain layer thickness d^*, the sum of the two types of losses reaches its minimum, resulting in the longest distance the SPs run along the metal-dielectric interface.

C. Way to Increase Precision of the SP Technique for Metal Dielectric Permittivity Determination in the THz Spectral Range

Because of an extremely high reflectivity of metals in the THz range, the methods based on measurements of radiation absorption, such as reflectometry and ellipsometry, cannot ensure necessary precision for determination of their dielectric permittivity. In contrast to the reflectivity-based methods, application of SPs for this aim looks more attractive as they interact with the sample on a long distance (thousands of λ) and their characters are fully determined by dielectric properties of the metal and the state of its surface.

The SP refractometry technique relies on measurements of the propagation length and phase velocity of the SPs guided by the sample surface that enables one to calculate both parts of the SP complex refractive index, and, solving the SP dispersion equation for a two-layer structure, find the required value of ϵ. Adequate arrangements for implementation of the technique were recently elaborated for samples of plane and cylindrical configurations [29,12].

What is strange is that the values of the metals ϵ obtained by the SP method in the THz spectral range are dramatically smaller as compared with those yielded by the techniques employing bulk radiation and those obtained by calculations with the Drude model [30]. The same contradiction was stated when the method realized with the time-domain spectroscopy technique was employed for ϵ evaluation of the highly doped silicon [31].

The question arises: what is the reason for this discrepancy? As mentioned in the Introduction, there are two main conjectures about the nature of the disagreement: (1) distinction in the dielectric properties of real metal surface and respective bulk crystal; (2) radiative losses of SPs on the roughness and intrinsic impurities of the surface.

The first conjecture is actual for any type of measurements with external radiation and cannot account for the disagreement between measurements with bulk and surface waves. The second conjecture seems more probable, but there was no experimental confirmation on the radiative losses' substantial impact to attenuation of THz SPs up to now.

Results of the paper presented clearly indicate that radiative losses play a very important role in attenuation of THz SPs, especially in case the metal surface is bare or is coated with a dielectric layer of thickness less than $\lambda/250$. There is no doubt that these losses diminish the THz SP propagation length L to a great extent, which should result in smaller values of the metal dielectric constant determined with the SP technique.

A way to increase precision of the SP refractometry technique becomes obvious as soon as one gives a glance at Fig. 9 and particularly at its inset. Divergence between calculated and measured values of L becomes smaller and smaller as the coating layer thickness d increases: for $d > \lambda/100$ the divergence is only twofold, whereas for $d < \lambda/300$, it exceeds a hundredfold. This means that in case the gold surface is coated with a ZnS layer of thickness $d > \lambda/100$, a measured L will be only two times less than its Drude model calculated counterpart; accordingly, a value of the dielectric permittivity of gold determined with the SP technique now will be much closer to its real magnitude as well as to its Drude model calculated value. The only charge "paid" for the precision increase of the method is deposition of a thicker layer, reliable knowledge of its thickness and the refractive index, and necessity to solve the SP dispersion equation for a three-layer structure instead of a two-layer one. We are going to implement this modified SP refractometry technique in the near future.

5. CONCLUSION

It has been experimentally demonstrated that radiative losses play an important role in the SP propagation along real metal surfaces at THz frequencies. The SP propagation length calculated by the Drude theory agrees well with experiments in the visible and near-IR ranges, but drastically disagrees with experiments in the THz region. To reveal the cause, we studied SPs

launched by monochromatic radiation of a free-electron laser with $\lambda = 130$ μm in "Au–ZnS layer–Air" plane structures with the layer thickness d of 0 to 0.025λ. Two sets of samples of different surface quality were studied. The measured decay length (penetration depth of SP field into air) with all the samples coincided with predictions of the Drude theory, which evidenced the validity of the theory in the THz range. Using imaging and Fourier-transform optical systems, we recorded the angular distributions of coupled and decoupled (radiative losses) waves traveling along the surface. It was found that radiative losses originating from transformation of SPs into BWs on surface imperfections can considerably exceed the Joule losses inside the metal (especially if the surface is uncovered) and were obviously responsible for the reduction in the THz SP propagation length. We discovered that with growing ZnS thickness the propagation length first increased, reached its maximum at $d \approx (0.003–0.004)\,\lambda$, and then monotonically decreased. The effect discovered proves the utility of covering a guiding surface with a thin dielectric layer as it enlarges the propagation length of THz SPs, concentrates the SP field in the proximity of the surface and protects it from outside intrusions, which is of great importance for THz SP communication lines.

Funding. Russian Science Foundation (RSF) (14-50-00080); Russian Foundation for Basic Research (RFBR) (16-32-00678); Fundamental Scientific Research (0069-2014-0014).

Acknowledgment. We thank the Siberian Synchrotron and Terahertz Radiation Centre (Novosibirsk) for the use of their equipment. The authors are thankful to G. N. Kulipanov and N. A. Vinokurov for encouraging the investigations, A. S. Kozlov and I. A. Azarov for their help in study of the samples, and the NovoFEL team for their assistance in the experiments.

REFERENCES

1. V. M. Agranovich and D. L. Mills, eds., *Surface Polaritons: Electromagnetic Waves at Surfaces and Interfaces* (Oxford University, 1982).
2. S. A. Maier, *Plasmonics: Fundamentals and Applications* (Springer, 2007).
3. O. Marti, H. Bielefeldt, B. Hecht, S. Herminghaus, P. Leiderer, and J. Mlynek, "Near-field optical measurement of the surface plasmon field," Opt. Commun. **96**, 225–228 (1993).
4. G. N. Zhizhin and V. A. Yakovlev, "Broad-band spectroscopy of surface electromagnetic waves," Phys. Rep. **194**, 281–289 (1990).
5. R. J. Bell, R. W. Alexander, C. A. Ward, and I. L. Tyler, "Introductory theory for surface electromagnetic waves spectroscopy," Surf. Sci. **48**, 253–287 (1975).
6. E. S. Koteles and W. H. McNeill, "Far infrared surface plasmon propagation," Int. J. Infrared Millim. Waves **2**, 361–371 (1981).
7. Z. Schlesinger, B. C. Webb, and A. J. Sievers, "Attenuation and coupling of far infrared surface plasmons," Solid State Commun. **39**, 1035–1039 (1981).
8. G. N. Zhizhin, E. V. Alieva, L. A. Kuzik, V. A. Yakovlev, D. M. Shkrabo, A. F. G. Van der Meer, and M. J. Van der Wiel, "Free-electron laser for infrared SEW characterization surfaces of conducting and dielectric solids and nm films on them," Appl. Phys. A **67**, 667–673 (1998).
9. G. D. Bogomolov, U. Y. Jeong, G. N. Zhizhin, A. K. Nikitin, V. V. Zavialov, G. M. Kazakevich, and B. C. Lee, "Generation of surface electromagnetic waves in terahertz spectral range by free-electron laser radiation and their refractive index determination," Nucl. Instrum. Methods Phys. Res. A **543**, 96–101 (2005).
10. J. Saxler, J. G. Rivas, C. Janke, H. P. M. Pellemans, P. H. Bolivar, and H. Kurz, "Time-domain measurements of surface plasmon polaritons in the terahertz frequency range," Phys. Rev. B **69**, 155427 (2004).
11. T.-I. Jeon and D. Grischkowsky, "THz Zenneck surface wave (THz surface plasmon) propagation on a metal sheet," Appl. Phys. Lett. **88**, 061113 (2006).
12. S. Pandey, S. Liu, B. Gupta, and A. Nahata, "Self-referenced measurements of the dielectric properties of metals using terahertz time-domain spectroscopy via the excitation of surface plasmon-polaritons," Photon. Res. **1**, 148–153 (2013).
13. M. Dragoman and D. Dragoman, "Plasmonics: applications to nanoscale terahertz and optical devices," Prog. Quantum Electron. **32**, 1–41 (2008).
14. H. Raether, *Surface Plasmons on Smooth and Rough Surfaces and on Gratings*, Vol. **111** of Springer Tracts in Modern Physics (Springer-Verlag, 1988).
15. E. D. Palik, ed., *Handbook of Optical Constants of Solids* (Academic, 1998).
16. I. S. Grigoriev and E. Z. Melikhov, eds., *Handbook, Physical Data* (Energoatomizdat, 1991) (in Russian).
17. M. A. Ordal, R. J. Bell, R. W. Alexander, L. L. Long, and M. R. Querry, "Optical properties of fourteen metals in the infrared and far infrared: Al, Co, Cu, Au, Fe, Pb, Ni, Pd, Pt, Ag, Ti, and W," Appl. Opt. **24**, 4493–4499 (1985).
18. Z. Schlesinger and A. J. Sievers, "IR surface-plasmon attenuation coefficients for Ge-coated Ag and Au metals," Phys. Rev. B **26**, 6444–6454 (1982).
19. G. N. Zhizhin, A. K. Nikitin, G. D. Bogomolov, V. V. Zavyalov, Y. U. Jeong, B. C. Lee, S. H. Park, and H. J. Cha, "Absorption of surface plasmons in 'metal-cladding layer-air' structure at terahertz frequencies," Infrared Phys. Technol. **49**, 108–112 (2006).
20. M. Gong, T.-I. Jeon, and D. Grischkowsky, "THz surface wave colapse on coated metal surfaces," Opt. Express **17**, 17088–17101 (2009).
21. G. N. Kulipanov, E. G. Bagryanskaya, E. N. Chesnokov, Y. Yu Choporova, V. V. Gerasimov, Y. V. Getmanov, S. L. Kiselev, B. A. Knyazev, V. V. Kubarev, S. E. Peltek, V. M. Popik, T. V. Salikova, M. A. Scheglov, S. S. Seredniakov, O. A. Shevchenko, A. N. Skrinsky, S. L. Veber, and N. A. Vinokurov, "Novosibirsk free electron laser—facility description and recent experiments," IEEE Trans. Terahertz Sci. Technol. **5**, 798–809 (2015).
22. V. V. Gerasimov, B. A. Knyazev, I. A. Kotelnikov, A. K. Nikitin, V. S. Cherkassky, G. N. Kulipanov, and G. N. Zhizhin, "Surface plasmon polaritons launched using a terahertz free electron laser: propagating along a gold-ZnS-air interface and decoupling to free waves at the surface tail end," J. Opt. Soc. Am. B **30**, 2182–2190 (2013).
23. G. I. Stegeman, R. F. Wallis, and A. A. Maradudin, "Excitation of surface polaritons by end-fire coupling," Opt. Lett. **8**, 386–388 (1983).
24. A. K. Nikitin, G. N. Zhizhin, and B. A. Knyazev, "A device to measure the propagation length of monochromatic surface electromagnetic waves of the infrared spectral range," Patent of Russia on Invention 2,470,269 (December 20, 2012).
25. K. Hasegawa, J. U. Nöckel and M. Deutsch, "Curvature-induced radiation of surface plasmon polaritons propagating around bends," Phys. Rev. A **75**, 063816 (2007).
26. M. Walther, D. G. Cooke, C. Sherstan, M. Hajar, M. R. Freeman, and F. A. Hegmann, "Terahertz conductivity of thin gold films at the metal-insulator percolation transition," Phys. Rev. B **76**, 125408 (2007).
27. A. F. Kay, "Scattering of a surface wave by a discontinuity in reactance," IRE Trans. Antennas Propag. **7**, 22–31 (1959).
28. I. Kotelnikov and G. Stupakov, "Dispersion relation of a surface wave at a rough metal-air interface," Phys. Rev. A (submitted).
29. V. V. Gerasimov, B. A. Knyazev, A. K. Nikitin, and G. N. Zhizhin, "A way to determine the permittivity of metallized surfaces at terahertz frequencies," Appl. Phys. Lett. **98**, 171912 (2011).
30. S. Pandey, B. Gupta, A. Chanana, and A. Nahata, "Non-Drude like behaviour of metals in the terahertz spectral range," Adv. Phys. X **1**(2), 176–193 (2016).
31. M. M. Nazarov, A. P. Shkurinov, F. Garet, and J.-L. Coutaz, "Characterization of highly doped Si through the excitation of THz surface plasmons," IEEE Trans. Terahertz Sci. Technol. **5**, 680–686 (2015).